ASTEROID DEBRIS: TEMPORARY CAPTURE AND ESCAPE ORBITS

MASSIMO VETRISANO, ALESSANDRA CELLETTI, AND GIUSEPPE PUCACCO

Abstract. We investigate the dynamical behaviour of debris ejected from the surface of an asteroid, due to a generic - natural or artificial - surface process. We make an extensive statistical study of the dynamics of particles flowing from the asteroid. We observe different behaviours: particles which fall again on the asteroid surface, or rather escape from its gravitational field or are temporary trapped in orbit around the asteroid. The tests are made by varying different parameters, like the size of the asteroid, its eccentricity, the angular velocity of the asteroid, the area-to-mass ratio of the debris.

We also extend the study to the case of a sample of binary asteroids with a mass ratio equal to 10^{-3}; we vary the distance of the moonlet from the asteroid, to see its effect on the debris dynamics.

Our simulations aim to identify regions where the debris can temporarily orbit around the asteroid or rather escape from it or fall back on the surface. These results give an important information on where a spacecraft could be safely stay after the end of the process which has produced the debris.

Keywords. Asteroid debris, temporary capture, escape orbits.

1. Introduction

During the last years space agencies have realized several robotic missions to asteroids. In one case (up to now), the probe *Philae* (within the ESA *Rosetta* mission) landed on the surface of the comet 67P/Churymov-Gerasimenko, thus providing the first in situ analysis of a comet. Among the future projects, space agencies started to envisage robotic, or even manned, missions to collect asteroid material and bring it back on the Earth. These projects might include a resurfacing of the asteroid, possibly due to ablation or other disruptive actions. At the light of future possible space missions, the study of the fate of the particles flowing from an asteroid has become of primary importance. However, such investigation is complicated by the fact that very often asteroids have irregular shapes, like those of the asteroids Castalia and Toutatis, which have been studied in [13], [14]. An obvious complication consists in establishing a good model for the shape of the asteroid, especially since it involves the computation of the main spherical harmonics which provide the asteroid's gravity field. On the other hand, the precision of the shape of the asteroid requires a large number of spherical harmonics, which in turn leads to very elaborated equations of motion (see also [4]).

The study of the orbital dynamics around irregular asteroids ([11], [13], [14], [15]) has shown the existence of a wide variety of behaviors, which - for our goals - we can group into three main classes: escape, impact and capture orbits. It is worth mentioning that the interplay of different forces, like the solar radiation pressure, the asteroid's gravity field, the solar attraction, has been investigated in [16] for dust particles ejected from the asteroid after a cratering impact. The stability of asteroid's ejecta has been analysed in [6] as the distance from the asteroid increases, leading to the conclusion that there exists a critical distance at which an abrupt transition between trapped and non trapped orbits occurs.

In this work we concentrate on a model which takes inspiration from the asteroid 65803 Didymos, a typical minor body which could be a possible target of space missions. However, some data have been necessarily modified to have significant effects on the dynamics on suitable (i.e., not too long) time scales. Beside its intrinsic interest, it is remarkable that Didymos has a moonlet at a relatively small distance. To encompass both cases of a single asteroid and of a binary system, we introduce two different models: the first one describes the motion of a particle under the influence just of the asteroid and the second one takes into account the presence of a moonlet. Taking into account these two models, we make an extensive statistical study as different parameters are varied, most notably the size of the asteroid, its orbital eccentricity, the area-to-mass ratio of the particle. We complement such study by the computation of the Lyapunov's exponents, which gives interesting information about the stability of the asteroid debris. The results show that a careful investigation of the debris dynamics around the asteroid is of seminal importance to decide where a spacecraft could be safely located, since it might happen that the debris is (temporarily) trapped in some regions around the asteroid, thus representing a concrete danger for the spacecraft (see also [2], [3], [5], [7], [10] for the study of the dynamics of space debris around the Earth).

This work is organized as follows. In Section 2 we present the equations of motion of the debris under the gravitational influence of the asteroid, the Sun and the solar radiation pressure. The case of an asteroid with a small moon is also considered. The experiments' settings, including the shape of the asteroid and the generation of the initial conditions of the test particles, are provided in Section 3. The results are presented in

Section 4, where we distinguish between temporary trapped orbits, escaping trajectories and particles falling back on the asteroid's surface. The case of a binary asteroid is analysed in Section 5. Some conclusions are drawn in Section 6.

2. The model

We consider an asteroid with mass m_A moving on a Keplerian orbit around the Sun with mass m_S; we denote by $\mu_A = \mathcal{G}m_A$, $\mu_S = \mathcal{G}m_S$ the corresponding gravity constants with $\mathcal{G}$ the gravitational constant. We assume that the asteroid has an ellipsoidal shape and that it rotates around an internal spin axis with angular velocity $\underline{\omega}$. Let $(S, \underline{I}, \underline{J}, \underline{K})$ be an inertial reference frame centred in the Sun and let $(A, \underline{i}, \underline{j}, \underline{k})$ be an asteroid body frame centred in the barycentre A of the asteroid (see Figure 1). The latter frame is more convenient to study the dynamics of a debris particle in the neighbourhood of the asteroid. The debris D is considered as a particle of mass m_d, much smaller than that of the primaries (asteroid and Sun); we assume that the debris moves in the gravitational field of the asteroid, subject to the interaction with the Sun and to the solar radiation pressure.

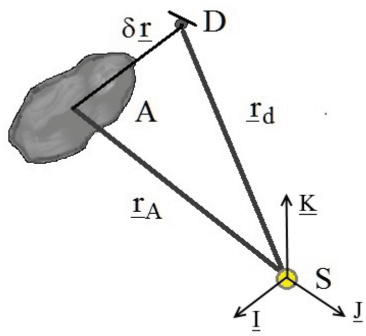

Figure 1. A debris D under the gravitational influence of an asteroid A and the Sun S.

2.1. **The equations of motion under the Sun-asteroid attraction.** We denote by $\delta\underline{r}$ the relative distance between the debris and the asteroid (compare with Figure 1) and by $\underline{u}$ the debris-Sun unit vector. The equations of motion of the debris can be written as (see [12])

$$\delta\ddot{\underline{r}} + 2\underline{\omega} \wedge \delta\dot{\underline{r}} + \underline{\omega} \wedge (\underline{\omega} \wedge \delta\underline{r}) = -\mu_A \, \frac{\delta\underline{r}}{\delta r^3} + \mu_S \, (\frac{\underline{r}_A}{r_A^3} - \frac{\underline{r}_d}{r_d^3}) + \frac{\partial U}{\partial(\delta\underline{r})} + F_{SRP}(r_d)\underline{u} \; , \quad (2.1)$$

where $\underline{r}_A$ and $\underline{r}_d$ are, respectively, the position vectors of the asteroid and the debris with respect to the Sun, U is the gravitational potential of the asteroid, where the gravity field of the asteroid is expressed as the sum of a spherical field plus higher order terms due to the ellipsoid shape of the asteroid. Explicit expressions for U as well as for the components of the equations of motion (2.1) are given in Appendix A. Finally, the term $F_{SRP}(r_d)$ denotes the solar radiation pressure, which depends on the distance r_d from the Sun through the expression

$$F_{SRP}(r_d) = C_r S_{SRP} (\frac{r_{1AU}}{r_d})^2 \frac{A_d}{m_d} \ , \tag{2.2}$$

where C_r is the reflectivity coefficient, S_{SRP} is the solar radiation pressure at distance[1] 1 AU, r_{1AU} is the equivalent of the astronomical unit in kilometres, A_d is the cross section area of the debris.

The Keplerian motion of the asteroid with respect to the Sun is governed by the equation

$$\delta\ddot{\underline{r}} = -\frac{\mu_S}{r_A^3}\ \underline{r}_A \ . \tag{2.3}$$

Equations (2.1) and (2.3), together with (2.2), are integrated in parallel to give the motion of the debris, while the asteroid moves around the Sun.

2.2. **Equations of motion with a small moon.** We also consider the case in which a moonlet orbits around the asteroid. In this case we need to modify the equations of motion (2.1) as follows:

$$\delta\ddot{\underline{r}} + 2\underline{\omega} \wedge \delta\dot{\underline{r}} + \underline{\omega} \wedge (\underline{\omega} \wedge \delta\underline{r}) = -\mu_A\ \frac{\delta\underline{r}}{\delta r^3} + \mu_S\ (\frac{\underline{r}_A}{r_A^3} - \frac{\underline{r}_d}{r_d^3}) + \frac{\partial U}{\partial(\delta\underline{r})} + F_{SRP}(r_d)\underline{u} + f_p(\delta\underline{r})\ ,$$

where the term f_p has been introduced in order to consider the perturbative effects due to another massive body, precisely a moonlet orbiting the asteroid. The explicit expression of such term is the following:

$$f_p(\delta\underline{r}) = \mu_m\ \left(\frac{\underline{r}_{d-moon}}{r_{d-moon}^3} - \frac{\underline{r}_m}{r_m^3}\right)\ ,$$

where μ_m is the gravity constant of the asteroid's moon, $\underline{r}_m$ is the position of the moon with respect to the asteroid reference frame, $\underline{r}_{d-moon} = \underline{r}_m - \delta\underline{r}$ is the position vector of the debris with respect to the moon.

[1]We recall that 1 AU (Astronomical Unit) corresponds to about 150 million km.

3. Experimental setup

In this Section we provide a description of the physical and dynamical assumptions on the asteroid (see Section 3.1) and we specify how the flow of particles originating from the asteroid is taken (see Section 3.2). The initial conditions of the moonlet are given in Section 3.3.

3.1. **Nominal case.** We consider an asteroid with triaxial shape; as a first case study, we take the semi-axes of the ellipsoid equal to $a = 5\ km$, $b = 3.65\ km$, $c = 2.45\ km$. This choice amounts to have that the moments of inertia I_1, I_2, I_3 are such that the equatorial oblateness of the ellipsoid is $(I_2 - I_1)/I_3 \simeq 0.3047$, while the second order coefficient of the gravity field is $J_2 \simeq 1/2(2I_3 - I_1 - I_2)/R_p^2 \simeq 0.2089$ (see Appendix A), where R_p is the mean radius of the ellipsoid.

As a prototype asteroid we consider an object which is similar in size and in the orbital elements to the asteroid 65803 Didymos, located at 1.64 AU with an eccentricity of circa 0.3839 and with a reduced inclination to the ecliptic about equal to 3.41^o. Its estimated diameter amounts to 0.75 km, but in the forthcoming discussion we will consider a larger asteroid to enhance its effects on the nearby particles. Didymos has a moonlet with an orbital period of 11.9 hr and moving at a distance from the asteroid's centre equal to a little more than three times the radius of Didymos.

As mentioned before, Didymos and its moonlet will serve as inspiration for the forthcoming study. Indeed, in the following simulations, the semi-major axis of the Keplerian orbit of the asteroid around the Sun is taken equal to $2.4599\ 10^8\ km$, while the eccentricity is fixed as $e = 0.3836$, and the inclination as $0.0595\ rad$. The argument of the perihelion is equal to $g = 1.2783\ rad$, the longitude of the ascending node is fixed to $\Omega = 5.5719\ rad$, while the true anomaly θ is taken as $\theta = 0$. We assume that the asteroid rotates around its shortest physical axis with angular velocity equal to $2.83\ 10^{-4}\ rad/s$; we also assume that the spin-axis is perpendicular to the orbit plane, thus neglecting the obliquity of the asteroid's rotation.

Beside the above nominal conditions, a number of test cases were considered by varying the following parameters:

- (i) we modify the shape of the asteroid and take its longest axis equal to $a = 10\ km$; this choice corresponds to consider a much more oblate body with asphericity parameter equal to $(I_2 - I_1)/I_3 \simeq 0.7649$ and with $J_2 \simeq 0.5067$;

(*ii*) we modify the trajectory of the asteroid and take it on a circular orbit around the Sun;

(*iii*) we consider different rotational states by taking a fraction, say $1/k$, of the angular velocity (precisely, we take $k = 1, ..., 10$);

(*iv*) we consider different values of the area-to-mass ratio, say 0.01, 0.005, 0.001, with a reflectivity coefficient equal to 1.3 (comprehensive of reflection and diffraction).

For each value of the rotational velocity and the area-to-mass ratio, a number of samples equal to 36 000 units was generated on the surface of the asteroid; they were taken from different locations and different velocities at the initial time. The orbit of each particle was then propagated up to 1 year.

3.2. **Particle's initial conditions.** The ejection of the particle from the surface of the asteroid is realized taking an initial velocity $\underline{v}_p$ composed by two parts:

$$\underline{v}_p = \underline{v}_t + v_\ell \underline{n} \ . \tag{3.1}$$

The tangential component $\underline{v}_t$ is given by the rotation of the asteroid around the smallest axis:

$$\underline{v}_t = \underline{\Omega}_a \wedge \underline{r}_s \ ,$$

where $\underline{\Omega}_a$ is the angular velocity of rotation of the asteroid and $\underline{r}_s$ denotes the initial position of the particle on the surface of the asteroid. As for the second component in (3.1), it is obtained by considering a fraction of the excess velocity, which allows to insert the debris into an escape trajectory ([13]):

$$v_\ell = k_e \left(-\underline{n} \cdot \underline{v}_t + \sqrt{(-\underline{n} \cdot \underline{v}_t)^2 + 2U_{Kep} - \underline{v}_t \cdot \underline{v}_t} \right) \ , \tag{3.2}$$

where k_e represents the fraction of the excess velocity (it is a number between 0 and 1), $\underline{n}$ denotes the unit vector which is normal to the surface at $\underline{r}_s$, U_{Kep} is the 2-body gravity potential at the position $\underline{r}_s$, namely $U_{Kep} = \mu_A/(\delta r)$ with $\delta r = |\delta \underline{r}|$.

We remark that the limit angular velocity, say Ω_{lim}, is computed as

$$\Omega_{lim} = \sqrt{\frac{2\mu_A}{a^3}}$$

at which the particles leaving the asteroid have zero energy, thus ensuring that the particles departing from the surface are not directly injected into an escape orbit. Then, denoting by $\Omega = |\underline{\Omega}|$, we consider the fractions

$$\Omega = \frac{1}{k} \Omega_{lim} \tag{3.3}$$

for $k = 1, ..., 10$.

In order to generate samples of particles flowing from different directions, we rotate randomly the second component in (3.1) around the normal direction with angles between $-\pi/2$ and $\pi/2$.

The trajectory of the particle is then propagated forward in time. The propagation stops in the case in which the particle falls back and impacts on the surface of the asteroid. On the contrary, the particle is considered to leave the orbit of the asteroid, when its Keplerian energy is positive (which implies that the particle has an orbital eccentricity greater than zero).

3.3. **Moonlet initial conditions.** The Moon around the asteroid is placed on a circular orbit with initial condition at distance r_m along the axis $\underline{x}_{hill}$ of the reference frame $(\underline{x}_{hill}, \underline{y}_{hill}, \underline{z}_{hill})$ with origin at the barycentre of the asteroid, $\underline{x}_{hill}$ along the orbital radius, $\underline{z}_{hill}$ along the orbital angular momentum and $\underline{y}_{hill}$ to form a right-handed reference frame. The initial velocity of the moonlet, say $\underline{v}_m$, is taken as

$$\underline{v}_m = \left(\sqrt{\frac{\mu_A}{r_m}}\ \underline{z}_{hill} \right) \times (r_m\ \underline{x}_{hill})\ .$$

The moonlet is assumed to be a sphere with radius R_m obtained by rescaling the radius R_A of the asteroid through the formula

$$R_m = \left(\frac{m_m}{m_A} \right)^{\frac{1}{3}}\ R_A\ ,$$

where m_m denotes the mass of the moonlet. When dealing with the binary system, asteroid-moon, we shall only consider the case with $a = 5\ km$.

4. Temporary capture and escape orbits

In this section we analyse the behaviour of the debris particles generated from the surface of the asteroid. In Section 4.1 we present some simulations providing the distribution of particles which fall back on the asteroid (the majority), those which escape from the gravitational attraction of the minor body (an almost negligible fraction) and the percentage of debris. In Section 4.2 we present some features of the dynamics obtained through the computation of the largest Lyapunov exponent, whose definition is briefly recalled in Appendix B.

4.1. **Evolution of the debris.** We consider an asteroid with semi-axes a, b, c, where b, c are fixed, precisely $b = 3.65\ km$, $c = 2.45\ km$, while we consider two cases for the larger semi-axis, namely $a = 5\ km$ and $a = 10\ km$. We study the case when the asteroid is on a circular orbit, $e = 0$, and when it is on an elliptic orbit with $e = 0.3836$. We take different rates of rotation by varying k in (3.3) as $k = 1, ..., 10$. Finally, we consider a particle with different values of the area-to-mass ratio: $A/m = 0.001, 0.005, 0.01\ m^2/kg$. Moreover, we take 100 values of k_e in (3.2) varying between 0.001 and 1.

The simulations on the evolution of the ejected particles are performed over one orbital period of the asteroid around the Sun, equal to 770 days.

Figure 2 provides the cumulative distribution of the surviving particles as a function of the distance from the asteroid. Different rotation rates are considered. Whenever the eccentricity and the area-to-mass ratio are small (Figure 2, top left panel), the particles are distributed at different distances from the asteroid. For example, for $k = 1$ about 90% of the particles are found at distance less than 200 km. For large eccentricities and/or large area-to-mass ratios, most of the surviving particles are found closer to the asteroid. Indeed, the bottom left panel of Figure 2 shows that 90% of the surviving particles are found below 300 km from the asteroid, while increasing the area-to-mass ratio (Figure 2, bottom right panel), the same percentage of particles is located below 180 km.

Next, we analyze in Figure 3 the case in which the biggest axis of the ellipsoidal shape of the asteroid is increased to $a = 10\ km$.

A comparison between Figures 2 and 3 shows that the increase of the largest asteroid radius provokes a spreading of the particles. For example, taking circular orbits and $A/m = 0.001\ km/m^2$ (Figures 3, top left panel), then most of the particles are found between 200 and 400 km. Such interval decreases (to $80 - 220\ km$) as the eccentricity and the area-to-mass ratio gets larger as in Figure 3, bottom right panel.

The overall survival rate at the end of one orbital period is synthetically shown in Figure 4, for $a = 5\ km$ (top panels), $a = 10\ km$ (bottom panels), $e = 0$ (left panels), $e = 0.3836$ (right panels) and different values of the area-to-mass ratio. The typical behaviour is that the survival rate is higher for larger values of A/m, thus showing that the solar radiation pressure perturbs the trajectories of the particles in such a way that a higher number evolves into non-impacting particles. Also the eccentricity helps to increase the survival, since it allows the trajectories to avoid an impact, soon after their ejection. Finally, the non-homogeneous gravity field affects the temporary capture of the particles, which are closer to the asteroid. In general, one finds more surviving particles on the long period for the case $a = 5\ km$, while for $a = 10\ km$ the survival rate is higher during the first 50 days.

4.2. **A dynamical exploration through Lyapunov exponents.** To get information about the stability of the particles surviving in orbit around the asteroid, we proceed

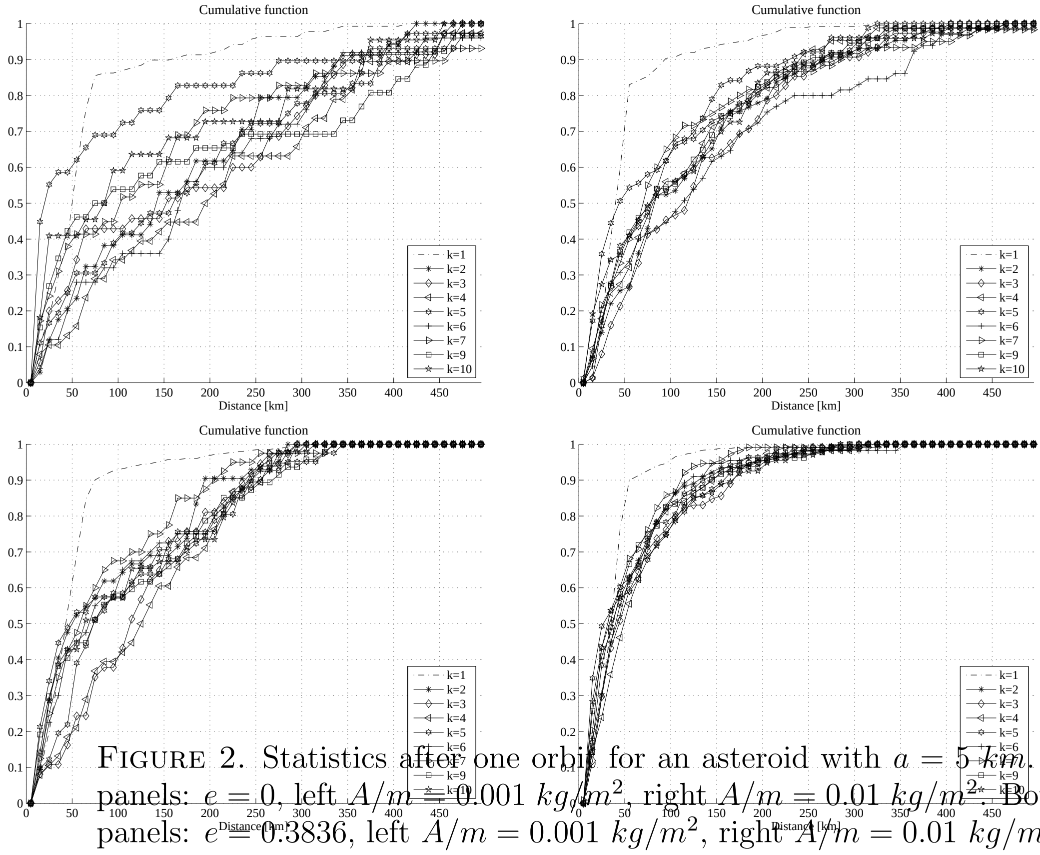

FIGURE 2. Statistics after one orbit for an asteroid with $a = 5\ km$. Top panels: $e = 0$, left $A/m = 0.001\ kg/m^2$, right $A/m = 0.01\ kg/m^2$. Bottom panels: $e = 0.3836$, left $A/m = 0.001\ kg/m^2$, right $A/m = 0.01\ kg/m^2$.

to compute the maximum Lyapunov exponent (see, e.g., [1]) for different values of k, say $k = 1, ..., 10$. The results on the Lyapunov exponents are complemented by a direct analysis of the orbital elements - semimajor axis, eccentricity, inclination - as a function of time (see Figure 5).

First, we show the survival rate as a function of k after a period of 10 000 days (see Figure 5) for $a = 5\ km$ (continuous line) and $a = 10\ km$ (dashed line); we also consider different values of the eccentricity and the area-to-mass ratio. As it is natural to expect, most of the particles fall back on the asteroid or rather escape from it. The situation is slightly better in the case $a = 10\ km$ and when the eccentricity is bigger; moreover, a larger number of particles survives when the effect of the solar radiation pressure is not big.

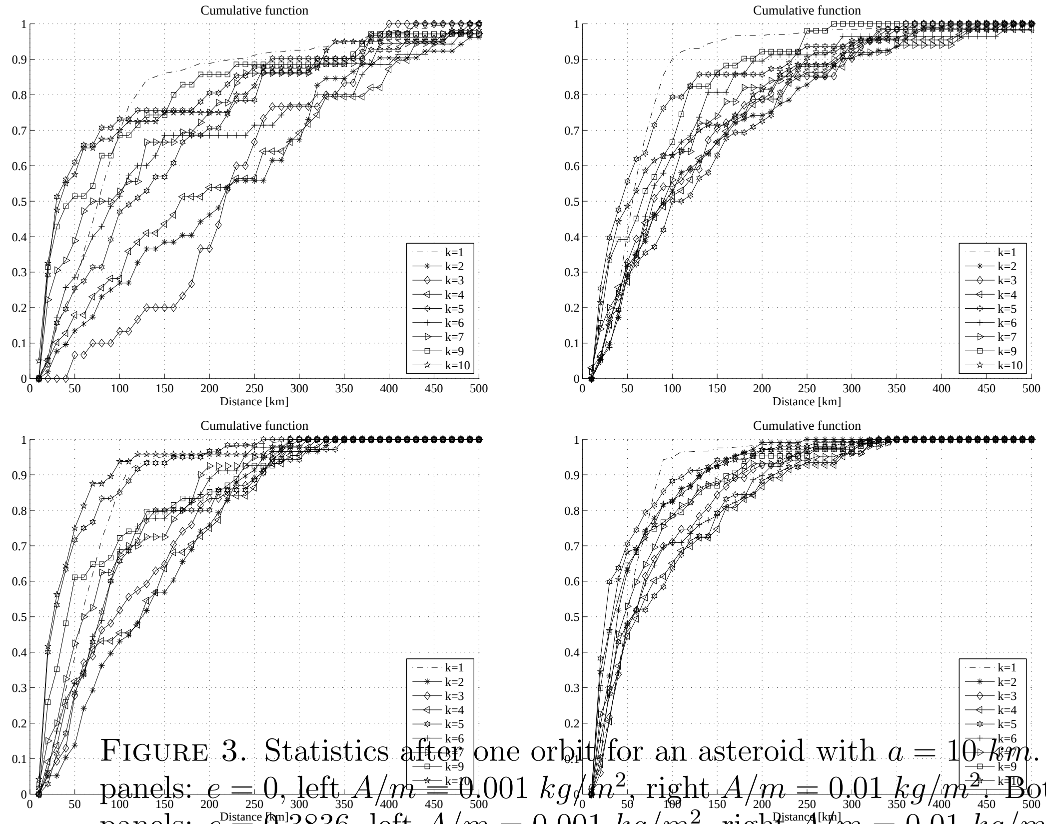

FIGURE 3. Statistics after one orbit for an asteroid with $a = 10\ km$. Top panels: $e = 0$, left $A/m = 0.001\ kg/m^2$, right $A/m = 0.01\ kg/m^2$. Bottom panels: $e = 0.3836$, left $A/m = 0.001\ kg/m^2$, right $A/m = 0.01\ kg/m^2$.

At the light of the results of Figure 5, we proceed to illustrate the determination of the Lyapunov's exponents for the case $k = 1$, which is the only relevant one in Figure 5. We performed several computations of the Lyapunov's exponents as the quantities a, e, A/m, k are varied. Among the different samples we analyzed, we present in Figure 6 the case of an asteroid with $a = 5\ km$, $e = 0.3836$ and $A/m = 0.005\ kg/m^2$ (top panels), which shows that after a (short) transient time the Lyapunov's exponents seem to tend to a finite positive value, thus denoting instability of several particles, although the eccentricity and the inclination remain bounded (top middle and right panels of Figure 6). When $a = 10\ km$, $e = 0.3836$, $A/m = 0.005\ kg/m^2$ (Figure 6, bottom panels), the number of unstable surviving particles increases, the Lyapunov's exponents

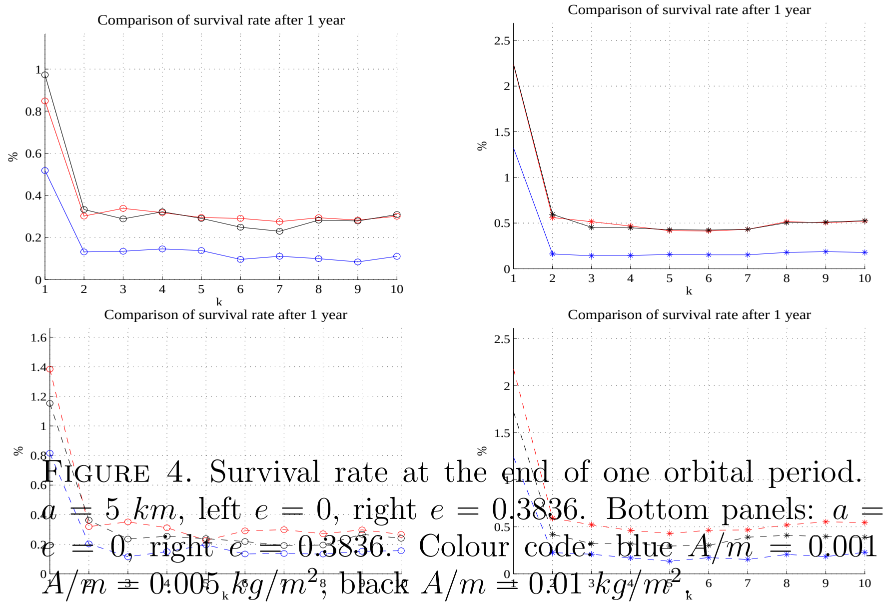

FIGURE 4. Survival rate at the end of one orbital period. Top panels: $a = 5\ km$, left $e = 0$, right $e = 0.3836$. Bottom panels: $a = 10\ km$, left $e = 0$, right $e = 0.3836$. Colour code: blue $A/m = 0.001\ kg/m^2$, red $A/m = 0.005\ kg/m^2$, black $A/m = 0.01\ kg/m^2$.

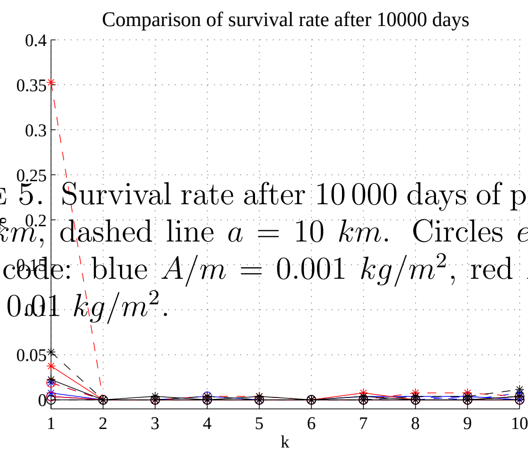

FIGURE 5. Survival rate after 10 000 days of propagation. Continuous line $a = 5\ km$, dashed line $a = 10\ km$. Circles $e = 0$, asterisks $e = 0.3836$. Colour code: blue $A/m = 0.001\ kg/m^2$, red $A/m = 0.005\ kg/m^2$, black $A/m = 0.01\ kg/m^2$.

tend again to a limiting value, but the eccentricity and the inclination vary on much larger intervals.

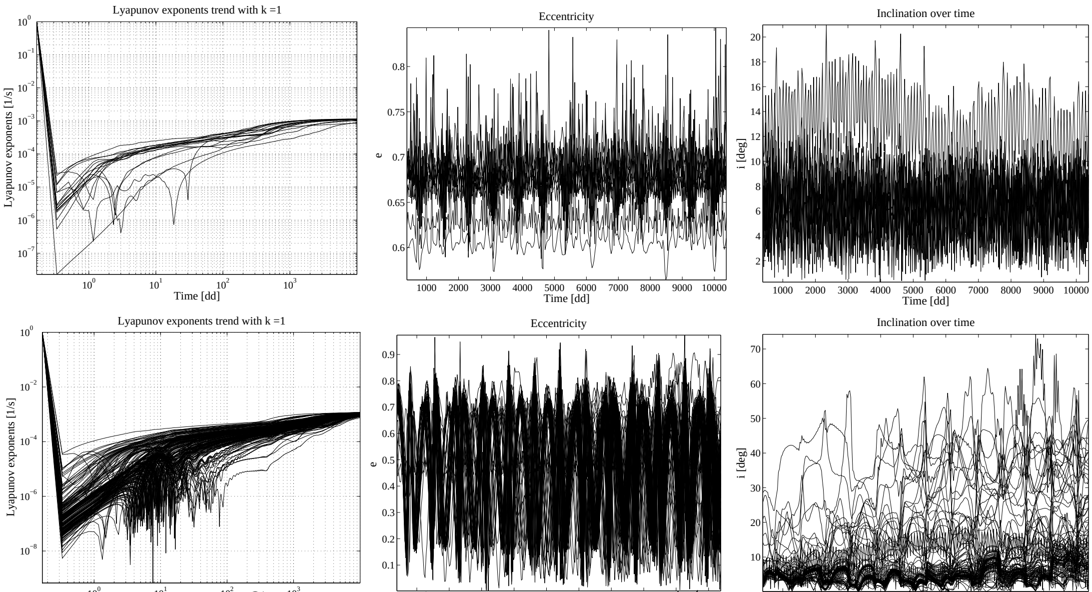

FIGURE 6. Case $a = 5$ km, $e = 0.3836$, $A/m = 0.005$ kg/m^2: top left Lyapunov exponent for $k = 1$, top middle eccentricity, top right inclination; bottom left Lyapunov exponent for $k = 1$, bottom middle eccentricity, bottom right inclination.

5. A binary asteroid

We now assume that the asteroid has a small companion, say a moonlet of negligible mass at distance r_m from the barycentre of the asteroid. Beside the variation's of the asteroid's larger axis, the eccentricity, the area-to-mass ratio, we perform several experiments using different distances between the asteroid and the moonlet, say $r_m = 15$, 25, 50, 100, 200 km. Figure 7 provides the cumulative distribution of the surviving particles for different values of the parameters. From the top panels we observe that the effect of the solar radiation pressure is to shrink the region where the particles can be found. In particular, for $A/m = 0.001$ kg/m^2, most of the particles are below 400 km, while for $A/m = 0.01$ kg/m^2 the particles are mainly found below 300 km.

The experiments show that the increase of the eccentricity further reduces the region where the particles can be found; for example, setting $e = 0.3836$, and keeping the other

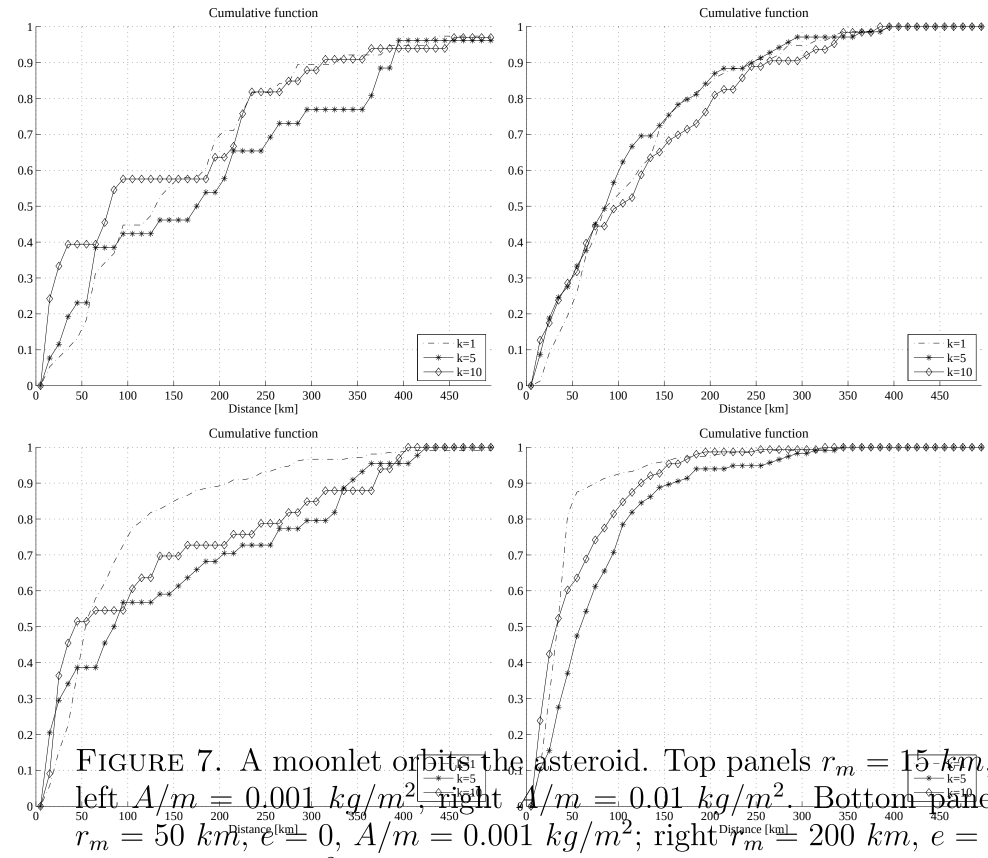

FIGURE 7. A moonlet orbits the asteroid. Top panels $r_m = 15\ km$, $e = 0$: left $A/m = 0.001\ kg/m^2$, right $A/m = 0.01\ kg/m^2$. Bottom panels: left $r_m = 50\ km$, $e = 0$, $A/m = 0.001\ kg/m^2$; right $r_m = 200\ km$, $e = 0.3836$, $A/m = 0.01\ kg/m^2$.

values as in the top right panel of Figure 7, the populated region decreases to 200 km from the asteroid. When the distance of the moonlet increases, as in the bottom panels of Figure 7, we notice that the moon tends to reduce its effect on the asteroid's debris. Indeed, the particles avoid the region close to the moon (Figure 7, bottom left panel), unless the eccentricity and the area-to-mass ratio are increased to counterbalance the effect of the moonlet (Figure 7, bottom right panel).

At high altitudes and without the moon, the gravitational influence of the Sun and the effect of the solar radiation pressure perturb the trajectories of the particles, possibly avoiding an impact with the asteroid. However, the presence of the moon breaks this situation and leads some particles to impact with the moon itself.

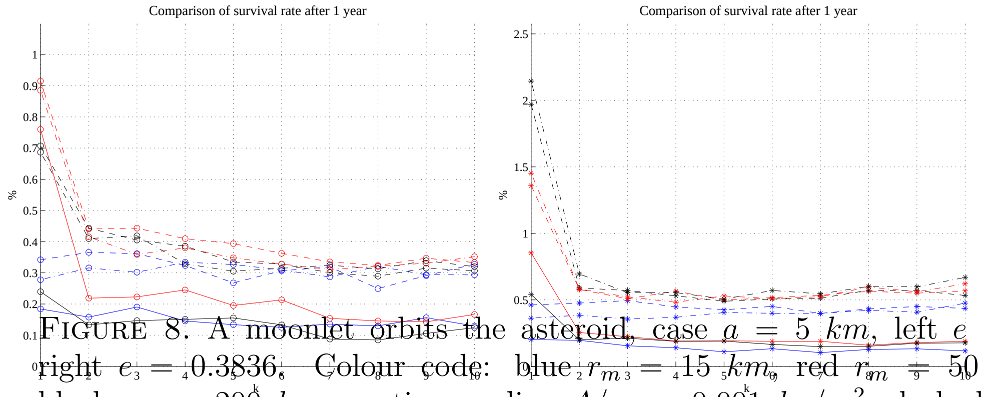

Figure 8. A moonlet orbits the asteroid, case $a = 5\ km$, left $e = 0$, right $e = 0.3836$. Colour code: blue $r_m = 15\ km$, red $r_m = 50\ km$, black $r_m = 200\ km$; continuous line $A/m = 0.001\ kg/m^2$, dashed line $A/m = 0.005\ kg/m^2$, dashed-dot line $A/m = 0.01\ kg/m^2$.

An overall picture of the survival rates is given in Figure 8, where the value $a = 5\ km$ is considered, while the eccentricity is set to zero in the left panel and to $e = 0.3836$ in the right panel. The plots summarize the results for different values of r_m and A/m. From Figure 8 we conclude that the region where the particles survive are mainly outside the asteroid-moon distance. When the moon is close to the asteroid, its effect is essentially to clean the space around the asteroid by most of the debris. In particular, the survival increases as the moonlet is more distant. When the moon is very far from the asteroid, then the statistics is close to that obtained by considering just the asteroid without the moon. The solar radiation pressure perturbs the trajectories of the particles, so that a higher number of particles avoids collision orbits, which might lead to an impact with the asteroid. Also the eccentricity allows to increase the survival rate, since its effect produces a perturbation of the trajectories, so that the particles will not impact soon after their ejection.

6. Conclusions

We study the dynamics of debris flowing from the surface of an asteroid, making a statistical study which leads to show different dynamical behaviors: an impact on the asteroid, an ejection or rather a temporary capture. The experiments are made by varying the most significative parameters, for example the shape of the asteroid, the eccentricity of its orbit, the area-to-mass ratio. Beside getting results by integrating of the equations of motion, we compute the largest Lyapunov's exponents to have information about the stability of those particles, which survive - at least temporarily - around the asteroid.

We also consider the effect of a small moonlet around the asteroid, which contributes to clean the environment, especially when it is not too far from the asteroid.

The issues raised in the present work should be considered as a basis for the investigation of asteroid's ejecta, in the sense that the methods presented here are very general and they can be implemented on specific cases. The results obtained in this paper suggest that the role of some parameters is particularly relevant. For example, we notice that an eccentric orbit of the asteroid helps to increase the survival rate, the same happens when increasing the area-to-mass ratio.

A detailed study of the dynamical behaviour of impact ejecta will be of foremost importance when designing a space mission to an asteroid; the techniques implemented in this paper can be applied to specific space missions to analyse the dynamics of the debris around the asteroid and to assess the possible effects of the debris on nearby spacecraft.

Acknowledgements. A.C. and G.P. were partially supported by the European MC-ITN grant Stardust and GNFM-INdAM. M.V. was supported by the European MC-ITN grant Stardust.

Appendix

A. The gravity potential

Following [9], the gravitational potential of an asteroid with mass m_A and radius R can be expressed as

$$U = \frac{\mathcal{G} m_A}{R} \sum_{n=1}^{\infty} \sum_{m=0}^{n} (C_{nm} V_{nm} + S_{nm} W_{nm}) \ ,$$

where V_{nm}, W_{nm} can be derived through recursive relations. After expanding in Legendre polynomials, one obtains the following formulae:

$$V_{00} = \frac{R}{r} \ , \qquad W_{00} = 0$$

and

$$\begin{aligned}
V_{mm} &= (2m-1)\Big(\frac{xR}{r^2}V_{m-1,m-1}-\frac{yR}{r^2}W_{m-1,m-1}\Big)\\
W_{mm} &= (2m-1)\Big(\frac{xR}{r^2}W_{m-1,m-1}+\frac{yR}{r^2}V_{m-1,m-1}\Big)\\
V_{nm} &= \frac{2n-1}{n-m}\frac{zR}{r^2}V_{n-1,m}-\frac{n+m-1}{n-m}\frac{R^2}{r^2}V_{n-2,m}\\
W_{nm} &= \frac{2n-1}{n-m}\frac{zR}{r^2}W_{n-1,m}-\frac{n+m-1}{n-m}\frac{R^2}{r^2}W_{n-2,m}\ ,
\end{aligned}$$

while C_{nm}, S_{nm} are the spherical harmonic coefficients ([9]), which describe the mass distribution of the asteroid.

Since we assume that the asteroid has an ellipsoidal shape with axes a, b, c, the moments of inertia are $I_1 = m_A(b^2+c^2)/5$, $I_2 = m_A(a^2+c^2)/5$, $I_3 = m_A(a^2+b^2)/5$. Therefore, we have that $S_{nm} = 0$, due to the symmetry of the ellipsoid, and

$$C_{20} = -J_2 = \frac{1}{m_A R^2}\frac{I_1+I_2-2I_3}{2}\ , \qquad C_{22} = \frac{1}{m_A R^2}\frac{I_2-I_1}{4}\ .$$

According to [9], the components of the acceleration just due to the potential U, say $\ddot{r}_U = (\ddot{x}_U, \ddot{y}_U, \ddot{z}_U)$, in an asteroid-fixed coordinate system, are given by the expansions

$$\ddot{x}_U = \sum_{n,m}\ddot{x}_{nm}^{(U)}\ , \qquad \ddot{y}_U = \sum_{n,m}\ddot{y}_{nm}^{(U)}\ , \qquad \ddot{z}_U = \sum_{n,m}\ddot{z}_{nm}^{(U)}\ , \tag{A.1}$$

where the most relevant terms in the series expansion (A.1) are the following:

$$\begin{aligned}
\ddot{x}_{20}^{(U)} &= -\frac{\mathcal{G}m_A}{R^2}C_{20}\ V_{31}\\
\ddot{y}_{20}^{(U)} &= -\frac{\mathcal{G}m_A}{R^2}C_{20}\ W_{31}\\
\ddot{z}_{20}^{(U)} &= -\frac{\mathcal{G}m_A}{R^2}C_{20}\ 3C_{20}\ V_{30}
\end{aligned}$$

and

$$\begin{aligned}
\ddot{x}_{22}^{(U)} &= \frac{\mathcal{G}m_A}{R^2}\ \frac{1}{2}\ \Big(-C_{22}V_{33}+2C_{22}V_{31}\Big)\\
\ddot{x}_{22}^{(U)} &= \frac{\mathcal{G}m_A}{R^2}\ \frac{1}{2}\ \Big(-C_{22}W_{33}-2C_{22}W_{31}\Big)\\
\ddot{z}_{22}^{(U)} &= \frac{\mathcal{G}m_A}{R^2}\ \Big(-C_{22}V_{32}\Big)\ .
\end{aligned}$$

B. The Lyapunov exponents

The Lyapunov exponent gives a measure of the chaotic character of the dynamics, as it provides the divergence of nearby trajectories. For a phase space of dimension n, there exist n Lyapunov exponents, although the largest one is the most significative.

A practical formula to compute the maximun Lyapunov exponent is the following ([8]):

$$\chi(\tau) \equiv \lim_{n\to\infty} \frac{1}{n\tau} \sum_{k=1}^{n} ln \frac{d(k\tau)}{d(0)} ,$$

where τ denotes the time step and $d(k\tau)$ is the distance at time $k\tau$ between trajectories at initial distance $d(0)$.

References

[1] A. Celletti, *Stability and Chaos in Celestial Mechanics*, Springer-Verlag, Berlin; published in association with Praxis Publishing Ltd., Chichester, ISBN: 978-3-540-85145-5 (2010)
[2] A. Celletti, C. Galeş, *On the dynamics of space debris: 1:1 and 2:1 resonances,* J. Nonlinear Science **24**, n. 6, 1231-1262 (2014)
[3] A. Celletti, C. Galeş, *A study of the main resonances outside the geostationary ring,* Advances in Space Research **56**, 388-405 (2015)
[4] A. Celletti, P. Negrini, *Non-integrability of the problem of motion around an oblate planet,* Celestial Mechanics and Dynamical Astronomy **61**, 253-260 (1995)
[5] T.A. Ely, K.C. Howell, *Dynamics of artificial satellite orbits with tesseral resonances including the effects of luni–solar perturbations*, Dynamics and Stability of Systems **12**, n. 4, 243-269 (1997)
[6] D.P. Hamilton, J.A. Burns, *Orbital stability zones about asteroids,* Icarus **92**, 118-131 (1991)
[7] A. Lemaître, N. Delsate, S. Valk, *A web of secondary resonances for large A/m geostationary debris,* Celest. Mech. Dyn. Astr. **104**, 383-402 (2009)
[8] L. Arnold, *Lyapunov exponents,* Lecture Notes in Mathematics, 1186 (1986)
[9] O. Montenbruck, E. Gill, *Satellite Orbits,* Springer-Verlag, Berlin, Heidelberg (2000)
[10] A. Rossi, *Resonant dynamics of Medium Earth Orbits: space debris issues,* Celest. Mech. Dyn. Astr. **100**, 267-286 (2008)
[11] K. Richter, H.U. Keller, *On the stability of dust particle orbits around cometary nuclei,* Icarus **114**, 355-371 (1995)
[12] D.J. Scheeres, *Orbital Motion in Strongly perturbed Environments. Applications to Asteroid, Comet and Planetary Orbiters,* 1st edition, Springer-Verlag, Berlin, Heidelberg (2012)
[13] D.J. Scheeres, S.J. Ostro, R.S. Hudson, R.A. Werner, *Orbits close to asteroid 4769 Castalia,* Icarus **121**, 67-87 (1996)
[14] D.J. Scheeres, S.J. Ostro, R.S. Hudson, E.M. DeJong, *Dynamics of orbits close to asteroid 4179 Toutatis,* Icarus **132**, 53-79 (1998)
[15] D.J. Scheeres, D.D. Durda, P.E. Geissler, *The fate of asteroid ejecta,* in Asteroids III, W.F. Bottke ed., Univ. Arizona Press, 527-544 (2002)
[16] D.J. Scheeres, F. Marzari, *Temporary orbital capture of ejecta from comets and asteroids,* Astron. Astroph. **356**, 747-756 (2000)

Flight Systems and Mission Analysis Business Unit, DEIMOS Space S.L.U., Ronda de Poniente, 19. Edificio Fiteni VI, portal 2 28760 Tres Cantos (Madrid), Spain
E-mail address: massimo.vetrisano@deimos-space.com

Department of Mathematics, University of Rome Tor Vergata, Via della Ricerca Scientifica 1, 00133 Roma (Italy)
E-mail address: celletti@mat.uniroma2.it

Department of Physics, University of Rome Tor Vergata, Via della Ricerca Scientifica 1, 00133 Roma (Italy)
E-mail address: pucacco@roma2.infn.it